EUROPEAN ORGANIZATION FOR NUCLEAR RESEARCH

CERN-EP/83-66
18 May 1983

LASER-ENHANCED ELECTRON-ION CAPTURE AND ANTIHYDROGEN FORMATION

R. Neumann[1)], H. Poth[2,*)], A. Winnacker[1)] and A. Wolf[2,*)]

1) Physikalisches Institut, Universität Heidelberg,
Federal Republic of Germany

2) Kernforschungszentrum Karlsruhe, Institut für Kernphysik,
Federal Republic of Germany

ABSTRACT

The electron-ion capture rate for low electron energies is calculated for various electron velocity distributions. Capture rates for electron-ion recombination stimulated by irradiation with light are evaluated. The results are applied to electron cooling and to positron-antiproton recombination to form antihydrogen. It is shown that laser-induced capture is a powerful method to study the electron cooling process and to maximize the antihydrogen rate. With this technique a pulsed antihydrogen beam of selectable energy and well collimated with an intensity of a few atoms per second can be anticipated.

(Submitted to Z. Phys.)

*) Visitor at CERN, Geneva, Switzerland

1. INTRODUCTION

The present paper is partly motivated by the fact that in the near future the Low Energy Antiproton Ring (LEAR) [1] will come into operation at CERN. Electron cooling will be an important part of that facility [2]. Moreover, the availability of a low energy antiproton beam may open up a possibility to produce, by radiative capture, antihydrogen atoms for spectroscopic studies.

The radiative capture of an electron by an ion

$$A^{+(n)} + e^- \rightarrow A^{+(n-1)} + h\nu$$

is an important process in the electron cooling of ion beams [3,4]. The analog reaction

$$\bar{p} + e^+ \rightarrow \bar{H} + h\nu$$

is the basic formation mechanism of antihydrogen.

Here we consider these processes in more detail with the idea of using them as diagnostics for the investigation of electron cooling [2]. Furthermore we are interested in the production of antihydrogen for precision experiments corresponding to those performed on the hydrogen atom. A promising direction for the latter is to overlap a stored antiproton beam with a low-emittance beam of positrons tuned to the same average velocity as the antiprotons [5]. Since this is similar to the electron cooling of a proton beam, all aspects of the antihydrogen formation can be studied in this process.

The capture of an electron (positron) can be stimulated by irradiation with light corresponding to a transition from the continuum into a bound atomic state

$$p + e^- + h\nu \rightarrow H + 2h\nu \ .$$

This opens up the possibility of studying in detail the cooling electron beam, particularly its velocity distribution, of enhancing the antihydrogen production rate, and of defining the final atomic state. Our consideration can also be applied to formation of other exotic atoms (e.g. $\bar{p}p$, e^+e^-, μ^+e^-, μ^-p, ...). In the following, we recall the basic principles of electron cooling before calculating the electron capture rates and we use our results for the application outlined above.

2. ELECTRON COOLING

The electron cooling technique is used to reduce momentum spread, divergence, and diameter of a stored ion beam (e.g. p, $\bar{p}$, ...). This is achieved by overlapping the ion beam over a certain length with a cold (i.e. monochromatic and low-emittance) electron beam of the same average velocity $v^* = \beta^* c$ (Fig. 1). The beams of particles with mass m can be characterized by temperatures T corresponding to their velocity spreads $\Delta = \sqrt{2T/m}$ in the coordinate system that is moving with the velocity v^*. (For the sake of simplicity, we put the Boltzmann constant k equal to one throughout the text and give the temperature in units of energy.)

In non-relativistic electron cooling electrons are generated by thermal emission from a hot cathode. Hence, they have a Maxwell velocity distribution whose width is given by the cathode temperature (typically T = 0.12 eV). The electrons are accelerated electrostatically to the desired energy (velocity). For sufficient high-voltage stability the longitudinal velocity spread as observed in the moving frame shrinks, while the transverse velocity spread remains unchanged. This situation is called *flattened* velocity distribution. The electron beam from cathode to collector is kept in a longitudinal solenoidal magnetic field to prevent the beam from blowing up on account of space-charge effects and in order to transform lateral electron movements (characterized by the transverse velocity) into cyclotron rotations about a magnetic-field line. The latter has the important consequence of effectively freezing the transverse electron motion, which leads to an enhancement of the cooling of small perturbations [6].

The cooling process can be understood as a heat exchange between the cold electron and the hot proton beam. When thermal equilibrium is reached the average velocity spread of the electrons Δ_e and of the ions Δ_i in the moving frame are related by $\Delta_i = \sqrt{m/m_i}\ \Delta_e$, with m and m_i being the mass of the electron and the ion, respectively. The mean relative velocity between electrons and ions is hence mainly determined by the electron velocity spread in that frame. The ions can be considered to be at rest in the electron gas. The electrons are populating a continuum band of width $T_e = (m/2)\ \Delta_e^2$ just above the ionization threshold of the ion (Fig. 2). Under

these conditions the electron-capture cross-section is large. In the case of protons, hydrogen atoms emerge from the cooling section and leave the storage ring tangentially (Fig. 1). This neutral beam contains a large amount of information about the proton- and electron-beam properties (e.g. temperature and alignment of the beams). In the following we calculate the formation rate.

3. SPONTANEOUS CAPTURE

The cross-sections for electron capture from the continuum into low-lying Coulomb bound states of hydrogen-like systems were calculated a long time ago [7]. For the final states of main quantum number n = 1, 2, 3 they are given in the Appendix and plotted in Fig. 3.

For low energies ($E_e << E_0$) the expressions for the cross-sections reduce to [7]:

$$\sigma_1 = 1.56\ \pi^2\ \alpha\ \lambda_e^2\ \frac{E_0}{E_e} = 1.676 \times 10^{-22}\ \frac{E_0}{E_e}\ [\mathrm{cm}^2]\ ,$$

$$\sigma_2 = 0.55\sigma_1\ ,\quad \sigma_{2s} = 0.15\sigma_1\ ,\quad \sigma_{2p} = 0.4\sigma_1\ , \tag{1}$$

$$\sigma_3 = 0.38\sigma_1\ ,\quad \sigma_{3s} = 0.05\sigma_1\ ,\quad \sigma_{3p} = 0.153\sigma_1\ ,\quad \sigma_{3d} = 0.177\sigma_1\ ,$$

where

E_e = kinetic energy of the electrons

E_0 = binding energy of the lowest atomic state (= $\frac{1}{2}\ Mc^2Z^2\alpha^2$)

$\lambda_e = \hbar/mc = 3.86 \times 10^{-11}$ cm = Compton wavelength of the electron

α = fine-structure constant.

Also shown in Fig. 3 are the curves for the less accurate cross-section as derived by Bethe and Salpeter [8], which is analytically given for all n by:

$$\sigma_n = 1.96\ \pi^2\ \alpha\ \lambda_e^2\ \frac{E_0^2}{nE_e(E_0 + n^2E_e)}\ . \tag{2}$$

As seen from Fig. 3, Eq. (2) agrees in the vicinity of $E_e = E_0$ with the full cross-section given by Stobbe [7]. At low energies, however, they differ by a factor of 0.8 for n = 1, by 0.88 for n = 2, and by 0.91 for n = 3.

Some important facts should be noted:

i) For high electron energies ($E_e > E_0$) preferentially low Coulomb states are formed.

ii) In the low-energy region, the capture cross-section increases for decreasing energies as v_e^{-2}. For radiative capture of electrons by protons one gets from Eq. (1):

$$v_e^2\sigma_1 = K_1 = 8.92\ [\text{mb}]\cdot c^2\ , \quad \text{with } K_1 = 1.56\ \pi^2\ \alpha\ \lambda\!\!\!^{-2}_e\ c^2\ 2E_0/mc^2 \tag{3a}$$

and from Eq. (2):

$$\lim_{v_e \to 0} v_e^2\sigma = K_n' = \frac{K_1'}{n} = \frac{11.2}{n}\ [\text{mb}]\ c^2\ , \quad \text{with } K_1' = 1.96\ \pi^2\ \alpha\ \lambda\!\!\!^{-2}_e\ c^2\ 2E_0/mc^2\ . \tag{3b}$$

iii) For $n \leq 3$ the population of states with high angular momentum ℓ is suppressed at high and favoured at low energies (as can be seen from Fig. 3).

iv) As shown recently (see, for instance, [9]), the population of ℓ sublevels reaches, for low energies and $n \geq 3$, a maximum at intermediate ℓ values and then falls off rapidly.

For a given electron velocity v_e the total spontaneous capture rate r^{spon} per ion (at rest) is

$$r^{spon} = n_e\ v_e \sum_{n=1}^{\infty} \sigma_n(v_e) \tag{4}$$

(where n_e = number of electrons per unit volume); it diverges for zero velocity. In general, electrons and ions can have particular velocity distributions. Then the capture cross-section has to be averaged with a normalized distribution function $f(\vec{v}_e - \vec{v}_i)$. In our case, however, $v_e >> v_i$ and the total capture rate is then

$$r^{spon} = n_e \int \sum_{1}^{\infty} f(\vec{v}_e) v_e \sigma_n(v_e)\ d^3\vec{v}_e = n_e \alpha_r\ , \tag{5}$$

where α_r is the recombination coefficient. We consider in the following a Maxwell distribution of the form

$$f(\vec{v}_e) = \frac{e^{-v_\perp^2/\Delta_\perp^2}\ e^{-v_\parallel^2/\Delta_\parallel^2}}{\Delta_\perp^2 \Delta_\parallel \pi\sqrt{\pi}}\ , \qquad \int f(\vec{v}_e)\ d^3\vec{v}_e = 1\ , \tag{6}$$

where ∥ denotes the velocity component along a given axis and ⊥ the projection of the velocity in the plane perpendicular to it. This form is chosen in order to allow for different temperatures $T_{\parallel}$ and $T_{\perp}$ in the longitudinal and transverse directions. In this case the capture rate is

$$r^{spon} = \frac{n_e}{\Delta_\perp^2 \Delta_\parallel \pi \sqrt{\pi}} \sum_1^\infty \int_0^\infty v_e \sigma_n(v_e) v_e^2 \, dv_e \int_0^{2\pi} d\phi \int_0^\pi \exp\left(-\frac{v_\perp^2}{\Delta_\perp^2} - \frac{v_\parallel^2}{\Delta_\parallel^2}\right) \sin\theta \, d\theta \ . \quad (7)$$

Integrating over ϕ and using $v_\perp^2 = v_e^2 \sin^2\theta$, $v_\parallel = v_e \cos\theta$, $x = \cos\theta$, we obtain

$$r^{spon} = \frac{4 n_e}{\Delta_\perp^2 \Delta_\parallel \sqrt{\pi}} \sum_1^\infty \int_0^\infty dv_e \, v_e \sigma(v_e) v_e^2 \, e^{-v_e^2/\Delta_\perp^2} \int_0^1 dx \exp\left[-x^2 v_e^2 \left(\frac{1}{\Delta_\parallel^2} - \frac{1}{\Delta_\perp^2}\right)\right] . \quad (8)$$

By introducing the error function

$$\text{erf}\ (z) = \frac{2}{\sqrt{\pi}} \int_0^z e^{-u^2} \, du = \frac{2}{\sqrt{\pi}} \sum_{n=0}^\infty \frac{(-1)^n}{n!} \frac{z^{2n+1}}{2n+1} \quad (9)$$

defining z and u as

$$z = v_e \sqrt{\frac{1}{\Delta_\parallel^2} - \frac{1}{\Delta_\perp^2}} \ , \quad u = xz \ , \quad (10)$$

this can be written as

$$r^{spon} = \frac{2 n_e}{\Delta_\perp^2 \Delta_\parallel} \sum_1^\infty \int_0^\infty dv_e \, v_e \sigma_n(v_e) v_e^2 \, e^{-v_e^2/\Delta_\perp^2} \frac{\text{erf}\ (z)}{z} \ . \quad (11)$$

For a spherical distribution ($\Delta_\perp = \Delta_\parallel$, $z = 0$) this results [by observing $\lim \text{erf}\ (z)/z = 2/\sqrt{\pi}$ for $z \to 0$] in:

$$r_s^{spon} = \frac{2 n_e}{\Delta_\perp^3} \frac{2}{\sqrt{\pi}} \sum_1^\infty \int_0^\infty dv_e \, v_e \sigma_n(v_e) v_e^2 \, e^{-v_e^2/\Delta_\perp^2} \ , \quad (12)$$

while for a flattened distribution [$\Delta_\parallel \ll \Delta_\perp$, $z = v_e/\Delta_\parallel$, erf $(v_e/\Delta_\parallel) \approx 1$] one finds:

$$r_f^{spon} = \frac{2 n_e}{\Delta_\perp^2} \sum_1^\infty \int_0^\infty dv_e \, \sigma_n(v_e) v_e^2 \, e^{-v_e^2/\Delta_\perp^2} \ . \quad (13)$$

Integration of Eqs. (12) and (13) is immediate for

$$\sigma_n(v_e)\, v_e^2 = \text{const} = K_n \tag{14a}$$

(which is a good approximation for $E_0 >> n^2 E_e$) and the partial capture rates are:

$$r_{s,n}^{spon} = \frac{2n_e}{\Delta_\perp} \frac{1}{\sqrt{\pi}} K_n \,, \qquad r_{f,n}^{spon} = \frac{2n_e}{\Delta_\perp} \frac{\sqrt{\pi}}{2} K_n \,, \qquad \frac{r_{f,n}^{spon}}{r_{s,n}^{spon}} = \frac{\pi}{2} \,. \tag{14b}$$

With Eqs. (1) one obtains, for spontaneous capture into specific final atomic states,

$$r_{1s}^{spon} : r_{2s}^{spon} : r_{2p}^{spon} : r_{3s}^{spon} : r_{3p}^{spon} : r_{3d}^{spon} = 100:15:40:5:15:18 \,, \tag{15}$$

independent of the shape of the velocity distribution for the low electron energies relevant here.

The total capture rate is calculated by evaluating the infinite sum in Eq. (11) with the appropriate cross-sections σ_n. This has been done by various authors [10,11]. We quote here the results of Bell and Bell [11] who evaluated the integral for the spherical Maxwellian as well as for the flattened distribution. They used essentially expression (2) for σ_n but applied a correction to the infinite sum over all n. Their results are

$$r_s^{spon} = \frac{2n_e}{\Delta_\perp} \frac{1}{\sqrt{\pi}} K_1' \left[0.43 + 0.48 \sqrt[3]{\frac{T_\perp}{E_0}} + \frac{1}{2} \ln \frac{E_0}{T_\perp} \right] = \frac{2n_e}{\Delta_\perp} \frac{1}{\sqrt{\pi}} K_s \,, \tag{16}$$

$$r_f^{spon} = \frac{2n_e}{\Delta_\perp} \frac{\sqrt{\pi}}{2} K_1' \left[1.12 + 0.278 \sqrt[3]{\frac{T_\perp}{E_0}} + \frac{1}{2} \ln \frac{E_0}{T_\perp} \right] = \frac{2n_e}{\Delta_\perp} \frac{\sqrt{\pi}}{2} K_f \,. \tag{17}$$

Here $T_\perp = (m/2)\, \Delta_\perp^2$ is the transverse electron energy (temperature). As already seen from (14b) the ground-state capture rate for a flattened distribution is a factor of $\pi/2$ higher than for a spherical distribution. The terms in the brackets result from the evaluation of the infinite sum and account for the electron capture into higher atomic levels. Their numerical values for $T_\perp = 0.2$ eV are 2.54 (3.23) for a spherical (flattened) distribution, hence

$$K_s = 2.54\ K_i' \ , \quad K_f = 3.23\ K_i' \quad (T_\perp = 0.2\ \text{eV}) \ . \tag{18}$$

This result indicates that in the case of a spherical (flattened) velocity distribution approximately 40% (30%) of all captures populate the ground state when the electrons have a transverse temperature of $T_\perp = 0.2$ eV.

4. COMPARISON WITH ELECTRON COOLING EXPERIMENTAL RESULTS

The calculations so far have been referring to the ion rest frame. To obtain the recombination rate per ion in the laboratory system the results have to be divided by $\gamma^{*2} = 1/(1-\beta^{*2})$. In electron cooling the electron beam overlaps with the ion beam only over a fraction η of the storage-ring circumference. Hence the total recombination rate for N_i circulating ions is

$$R = r^{spon}\ \frac{\eta}{\gamma^{*2}}\ N_i \ . \tag{19}$$

In electron cooling experiments at Novosibirsk [12] a recombination coefficient α_r [see definition (5)] of 2.26×10^{-12} cm^3 s^{-1} was found [13]. Independent measurements point to a transverse temperature of about 0.2 eV in these experiments. Using this value we find [Eqs. (16), (17)]:

for a flattened distribution: $\alpha_r^f = 2.2 \times 10^{-12}$ cm^3 s^{-1} (20)

for a spherical distribution: $\alpha_r^s = 1.14 \times 10^{-12}$ cm^3 s^{-1} . (21)

Hence the experimental result from Novosibirsk is in agreement with the assumption of a flattened distribution for a transverse temperature $T_\perp = 0.2$ eV, which is reasonable in view of the experimental conditions as analysed in Ref. 12. Moreover the ICE results [4] are in good agreement with the recombination rate obtained for a flattened distribution.

5. LASER-INDUCED CAPTURE

Electron capture can be enhanced through the presence of electromagnetic radiation via stimulated emission. Through spontaneous recombination all atomic levels are populated and electrons of any velocity are involved. In stimulated

capture, however, only atomic levels of the same main quantum number are reached and only electrons within the velocity interval $[v_0 - \Delta v/2,\ v_0 + \Delta v/2]$ can participate as imposed by energy conservation:

$$\frac{mv_0^2}{2} + \frac{E_0}{n^2} = h\nu \ , \qquad \Delta v \simeq \frac{h}{mv_0}\,\Delta\nu \ , \tag{22}$$

where ν is the frequency of the (absorbed) emitted photon and $\Delta\nu$ is the combined spectral width of the radiation field and the natural width of the bound atomic state.

The ratio g of induced (W^{ind}) to spontaneous (W^{spon}) recombination probability is

$$g = \frac{W^{ind}}{W^{spon}} = u(\nu)\,\frac{B}{A} \ , \tag{23}$$

where

$$u(\nu) = \frac{P}{cF\Delta\nu} \tag{24}$$

is the spectral energy density of the radiation field of power P and photon beam cross-section area F. The quantities A and B are the Einstein coefficients for spontaneous and stimulated emission, respectively, which are related by

$$A = 8\pi\,\frac{h\nu^3}{c^3}\,B \ . \tag{25}$$

From Eqs. (23), (24), and (25), one gets

$$g = \frac{Pc^2}{F\Delta\nu 8\pi h\nu^3} \ . \tag{26}$$

Another way to obtain Eq. (26) is by recalling that according to the basics of radiation theory $g = N(\nu)$, where $N(\nu)$ is the number of photons per mode present at frequency ν. This $N(\nu)$ is calculated as follows: for a laser power P the number of photons n_ν in the interaction volume V is $n_\nu = PV/(cFh\nu)$. The number of modes in V within the frequency interval $\Delta\nu$ is $n_m = 8\pi V\nu^2\Delta\nu/c^3$. By distributing the available photons equally over the available modes one gets

$$g = N(\nu) = \frac{n_\nu}{n_m} = \frac{Pc^2}{F\Delta\nu 8\pi h\nu^3} ,$$

in agreement with Eq. (26). Thus g is the enhancement factor for induced capture of electrons within the above-defined velocity interval into an atomic bound state $r_n^{ind}(\Delta v)$ compared to spontaneous capture of electrons out of the same interval into the same atomic level $r_n^{spon}(\Delta v)$. The total gain G, which is the ratio of induced capture to *all* spontaneous captures, is hence obtained by multiplying g by the ratio of spontaneous captures of electrons within the velocity interval to all spontaneous captures:

$$G \equiv \frac{r_n^{ind}(\Delta v)}{r^{spon}} = g \frac{r_n^{spon}(\Delta v)}{r^{spon}} . \tag{27}$$

The total recombination rate is then

$$r^{tot} = r^{spon} (1+G) . \tag{28}$$

$r_n^{ind}(\Delta v)$ is obtained by integrating in Eq. (11) only the term n of the infinite sum over the proper velocity interval:

$$r_n^{ind}(\Delta v) = g r_n^{spon}(\Delta v) = \frac{Pc^2}{8\pi h\nu^3 F\Delta\nu} \frac{2n_e}{\Delta_\perp^2 \Delta_\parallel} \int_{v_0-\Delta v/2}^{v_0+\Delta v/2} dv_e \, v_e \sigma_n(v_e) v_e^2 \, e^{-v_e^2/\Delta_\perp^2} \frac{\mathrm{erf}(z)}{z} . \tag{29}$$

In order to understand the dependence of G on v_0 and $\Delta_\parallel, \Delta_\perp$ we consider again the two extreme cases of a spherical and a flattened velocity distribution and replace $\sigma_n(v_e)v_e^2$ by its low-velocity limit K_n'. We further consider $\Delta v \ll v_0$. Then the integral in Eq. (29) can be replaced by the integrand at $v_e = v_0$ multiplied by $\Delta v = h\Delta\nu/(mv_0)$. For a spherical distribution [using Eqs. (14), (16), and $\mathrm{erf}(z)/z = 2/\sqrt{\pi}$] this results in

$$G_s = \frac{Pc^2}{8\pi\nu^3 F} \frac{e^{-v_0^2/\Delta_\perp^2}}{T_\perp} \frac{K_n'}{K_s} , \tag{30}$$

For a flattened distribution one obtains in the same way [using Eqs. (14), (17), and $z \simeq v_e/\Delta_\parallel$]:

$$G_f = \frac{Pc^2}{8\pi\nu^3 F} \frac{\Delta_\perp}{v_0} \frac{e^{-v_0^2/\Delta_\perp^2}}{T_\perp\sqrt{\pi}} \frac{K_n'}{K_f} \operatorname{erf}\left(\frac{v_0}{\Delta_\parallel}\right) . \tag{31}$$

For $v_0 \leq \Delta_\parallel$, $G_f \propto \Delta_\perp/\Delta_\parallel$, since $\operatorname{erf}(v_0/\Delta_\parallel) \simeq 2v_0/(\sqrt{\pi}\Delta_\parallel)$. Comparing Eqs. (30) and (31) one finds, moreover, that for $v_0 \leq \Delta_\parallel$

$$G_f = \frac{2}{\pi} G_s \frac{\Delta_\perp}{\Delta_\parallel} \frac{K_s}{K_f} . \tag{32}$$

This shows that a flattened velocity distribution of the electrons would considerably enhance induced recombination if the radiation frequency was chosen such that electrons with velocities less than $\Delta_\parallel$ are captured. Of course G_f does not increase unlimitedly with decreasing $\Delta_\parallel$ since in this consideration the conditions $\Delta v \ll v_0 \leq \Delta_\parallel$ have to be fulfilled. This means that the difference between the energy of the laser light and the electron binding energy after capture E_0/n^2 has to be smaller than $T_\parallel$ and that the spectral width $h\Delta\nu$ of the optical transition is much smaller than $T_\parallel$. In practice this is fulfilled, since electron beams can hardly be frozen in the longitudinal temperature such that they could encounter this limit.

6. NUMERICAL ESTIMATES FOR RECOMBINATION IN ELECTRON COOLING

Let us consider electron capture stimulated by irradiating the electron-ion gas with a laser beam of suitable frequency. Using Eq. (22) to express ν, bearing in mind that $K_s = 2.54\ K_1'$ [Eq. (18)] holds for the typical value $T_\perp = 0.2$ eV, and putting $K_n' = K_1'/n$ [Eq. (3b)] we can rewrite Eq. (30) for $v_0 \ll \Delta_\perp$:

$$G_s = \frac{P\pi^2 n^5}{cF} \left(\frac{\hbar c}{E_0 + n^2 m v_0^2/2}\right)^3 \frac{1}{T_\perp} \frac{1}{2.54} . \tag{33}$$

Thus again with $T_\perp = 0.2$ eV and with a laser beam of intensity $I = P/F$, we obtain for electron capture on protons into the $n = 2$ level ($E_0 \gg 2mv_0^2$):

$$G_s = 0.4\ I/(\mathrm{MW \cdot cm^{-2}}) . \tag{34}$$

In electron cooling, flattened distributions with $\Delta_\perp/\Delta_\parallel \geq 30$ can be anticipated, which increases the gain per MW of laser power for a flattened distribution and $v_0 \leq \Delta_\parallel$ to

$$G_f \geq 6\ I/(\mathrm{MW\ cm^{-2}})\ . \tag{35}$$

The useful laser power is, however, limited as we shall see in the following.

7. THE ROLE OF PHOTOIONIZATION AND FREE-FREE TRANSITIONS IN INDUCED RADIATIVE CAPTURE

In the following two processes will be considered which could upset the concept of enhancing radiative capture by stimulated emission.

7.1 Photoionization

If the electron has been captured by the proton into a bound state of a hydrogen atom in the presence of light, it may happen that the light immediately reionizes the atom. It will turn out that this process puts an upper limit on the laser power which should reasonably be applied. We shall give an estimate of this limit.

The cross-sections for photoionization σ^{ph} from hydrogen states n = 1 and n = 2 are tabulated [7] and have a magnitude of the order of $\sigma^{ph} \approx 10^{-17}\ \mathrm{cm^2}$. The photoionization rate for one hydrogen atom is

$$Z^{ph} = \phi\sigma^{ph}\ , \tag{36}$$

where $\phi = P/(Fh\nu)$ is the photon flux. If the atom is exposed to the light field during a time τ, the relation $Z^{ph}\tau = \phi\sigma^{ph}\tau \leq 1$ must hold and therefore ϕ has to be:

$$\phi \leq \frac{1}{\tau\sigma^{ph}} \tag{37}$$

in order to ensure that the atom formed is not reionized again. With a value of τ of the order of a few nanoseconds (either determined by the lifetime of the atomic state or by the laser pulse duration), say $\tau \simeq 3$ ns, one gets

$$\phi \leq 3.3 \times 10^{25}\ \mathrm{photons\ cm^{-2}\ s^{-1}}\ . \tag{38}$$

This maximum useful photon flux limits the radiation intensity I for transitions to the n = 2 level ($h\nu$ = 3.4 eV) to 18 $MW \cdot cm^{-2}$. For the spherical distribution we obtain from Eq. (34)

$$G_s^{max} = 7.2 \ . \tag{39}$$

For a flattened distribution with $\Delta_\perp/\Delta_\parallel \approx 30$ this would increase by a factor of 15 [see Eq. (32)]; hence

$$G_f^{max} = 110 \tag{40}$$

seems feasible.

The limit for the useful photon flux, Eq. (38), and the corresponding useful laser power density are well in the range of dye lasers pumped by modern excimer lasers.

It should finally be noted that in the case of a relativistic beam ($\beta^* \approx 0.5$) relativistic corrections should be applied. For the precision we aim at in these calculations those corrections have been neglected.

7.2 Free-free transitions

Another process to be considered is the following one: instead of inducing a transition of the free electron into a bound state the light could excite the electron to a higher continuum state. The cross-section for a photon of energy $h\nu$ to be absorbed in such a free-free transition is given by an average over the electron velocity distribution:

$$\sigma^{ff}(\nu) = n_e \int \sigma^{ff}(v_e,\nu) f(\vec{v}_e) d^3\vec{v}_e \ . \tag{41}$$

Following the discussion in Section 78 of [8], we use

$$\sigma^{ff}(v_e,\nu) = \frac{c^2}{8\pi\nu^3} \cdot \frac{16}{3} \alpha \lambda_e^2 c^2 \frac{2E_0}{mc^2} \cdot \frac{1}{v_e} \cdot \frac{\pi}{\sqrt{3}} \tag{42}$$

(see Eqs. 78.13, 78.11, 78.10 in Ref. 8), which should be accurate to within 20% in our case ($E_e << E_0$, $h\nu \approx E_0/n^2$, n = 2). By averaging as above (Section 3) and multiplying (41) with the photon flux, we calculate the following rates of free-free transitions for the spherical and flattened distributions:

$$r_s^{ff} = \frac{Pc^2}{8\pi\nu^3 F}\,\frac{1}{h\nu}\,\frac{16\pi}{3\sqrt{3}}\,\alpha\lambda_e^2 c^2\,\frac{2E_0}{mc^2}\cdot\frac{2n_e}{\Delta_\perp}\cdot\frac{1}{\sqrt{\pi}}\ ,$$

$$r_f^{ff} = \pi/2\cdot r_s^{ff}\ . \tag{43}$$

These rates have to be compared with the rates for induced capture, $r_n^{ind} = G\cdot r^{spon}$. For the worst case of a spherical velocity distribution, we obtain using Eq. (30) for ($v_0 \ll \Delta_\perp$), and Eqs. (16) and (3b):

$$\frac{r_s^{ff}}{r_{s,n}^{ind}} = \frac{16\pi/(3\sqrt{3})}{1.96\ \pi^2}\ nT_\perp/(h\nu) = 0.55\ nT_\perp/(h\nu)\ . \tag{44}$$

This ratio equals 0.06 for n = 2 and $T_\perp$ = 0.2 eV. It is seen that photon absorption due to free-free transitions is less important than induced capture into lower bound states thanks to the relatively low electron temperature, and can still be neglected in our case.

8. INDUCED CAPTURE AS DIAGNOSTICS FOR ELECTRON COOLING

Owing to the large gain factor for induced capture and its simple dependence on $\Delta_\perp$ and $\Delta_\parallel$, the observation of stimulated recombination provides an excellent means to determine directly these important quantities in electron cooling. As is obvious from Eqs. (30), (31) and (32), the effective transverse electron temperature can be measured from the decreasing rate of G as a function of v_0. The longitudinal electron temperature can be determined from the plateau value of the gain for small v_0 [Eq. (31)].

Experimentally this is realized by shooting a laser beam antiparallel to the electron and ion beams into the cooling region. In this way advantage can be taken of the fact that the laser light is shifted to a shorter wavelength in the electron-ion rest frame owing to the Doppler effect:

$$\lambda = \lambda_{lab}(1 + \beta^* \cos\theta_{lab})\ \gamma^*\ , \tag{45}$$

where

θ_{lab} is the angle between laser and electron (ion) beam.

The frequencies can be matched by suitably adjusting β^*. The electron velocity distribution can be scanned by tuning the laser frequency, or by varying β^* and measuring the recombination rate during the laser pulse duration. Note in passing that in this way the velocity of the ion beam can be measured very precisely. For instance, for a cooled proton beam of 10^{10} particles circulating with $\beta^* = 0.47$, an electron density of 10^8 cm^{-3}, a transverse electron energy of $T_\perp = 0.2$ eV, and an overlap length of 2% of the ring circumference, we would expect a spontaneous H-formation rate of [Eqs. (19) and (20)]:

$$R_H = 4 \times 10^4 \quad s^{-1} \ .$$

Using a laser of sufficient power we can achieve a gain of, let us say, G = 100 for induced capture in n = 2 levels. Assuming a laser pulse duration of 10 ns and a repetition rate of 10 Hz, this results in a signal rate of about 0.4 s^{-1}, when counting only during the laser-on period at a signal-to-noise ratio of G.

9. APPLICATION TO THE FORMATION OF ANTIHYDROGEN

This application has been discussed in an earlier paper [5] which also included an estimate of the role that laser-induced radiative capture may play in this context.

Antihydrogen would be the first antiatom ever produced. It would provide -- by comparison with existing high-precision data on normal hydrogen -- an opportunity to investigate questions related to matter-antimatter symmetries, and would allow in particular for tests of quantum-electrodynamics in a system of bound antiparticles. It would open up the possibility to study the interaction of hydrogen and antihydrogen atoms, a repeatedly discussed problem [14]. Furthermore, since this system is electrically neutral, experiments may be conceived to test the interaction of antimatter with the gravitational field.

Basically two concepts have been developped in [5] for application in LEAR [1]. They differ in the way the positron beam required for antihydrogen formation is produced. One consists in the following scheme (fig. 4): the highest possible intensity of $\bar{p}$ is stored and cooled in LEAR (5×10^{11} $\bar{p}$). Bursts of about 10^6 e^+, of 25 ns length, are produced at a rate of 1 s^{-1} by a 20 MeV linac. These pulses are injected into an e^+ storage ring. There, the positrons are cooled by stochastic cooling, decelerated to the interaction energy, and then further cooled by electron cooling. In such a scheme positron densities of $n_{e+} \simeq 200$ cm^{-3} can be expected at a temperature of about 0.3 eV. We then apply (19) to calculate the total recombination rate $R_{\bar{H}}$. In the above scheme, η is about 0.06 and $r_s^{spon} = 1.73 \times 10^{-10}$ [Eq. (16) for $T_\perp = 0.3$ eV]. One gets (for $\gamma = 1.15$)

$$R_{\bar{H}} = 4\ \bar{H}\ s^{-1}\ . \tag{46}$$

In this scheme a continuous beam of $\bar{H}$ is produced. The method of induced radiative capture would not be applicable in this case, because, as discussed above, it requires laser powers of the order of some MW which are only available during laser pulses.

The second scheme discussed in [5] relies on the rapid progress taking place in the techniques of positron thermalization and bunching [15]. In these techniques, use is made of the fact that positrons from a radioactive source or a linac conversion target may be thermalized on metal surfaces. This may be applied to produce cooled beams of positrons, which at the same time can be focused and bunched to pulses of a few ns length. These thermalized positrons subsequently would be reaccelerated to the energies required for the recombination with the antiprotons in LEAR. The reacceleration provides a flattened positron velocity distribution. The positron density in a bunch would be

$$n_{e+} = \frac{N_{e+}}{\beta c \tau F}\ ,$$

where N_{e+} is the number of positrons in the bunch and F its cross-section. With a repetition rate of f pulses per second, we get a mean positron density of

$$n_{e+} = \frac{N_{e+}}{\beta c F} \cdot f\ . \tag{47}$$

With $N_{e^+} = 10^7$, $\beta = 0.3$, $F \simeq 0.1$ cm^2, $\eta = 0.06$, and $f = 100$ s^{-1} this gives $n_{e^+} \simeq 1.1$ cm^{-3}. In this case one gets [for $\alpha_r^f = 2.2 \times 10^{-12}$ cm^3 s^{-1}, see (20)]:

$$R_{\bar{H}} \simeq 0.06\ \bar{H}\ s^{-1} .$$

So, even if the fairly optimistic assumptions concerning the developments in positron thermalization turn out to be founded, the production rate $R_{\bar{H}}$ would be about two orders of magnitude smaller than in the first scheme [see Eq. (46)]. However, here the $\bar{H}$ are produced in bunches of a few ns length. This opens up the possibility to apply the technique of laser-induced radiative capture. As a matter of fact, according to Eq. (40) this technique may just provide the missing two orders of magnitude, making the second scheme competitive. The second scheme, moreover, is more desirable, because the antihydrogen atoms would be produced in pulses at a well-defined time, which considerably facilitates subsequent spectroscopic experiments. The radiative capture, by the way, would already constitute in itself a first spectroscopic experiment.

10. SUMMARY AND CONCLUSION

We first recalled the main aspects of spontaneous electron-ion capture for a spherical Maxwellian and a flattened electron velocity distribution. Theoretical calculations are in good agreement with experimental data from electron cooling experiments as far as available.

We have considered the stimulation of electron capture on ions by light and calculated the enhancement with respect to spontaneous recombination. It was shown that an instantaneous increase of captures by some orders of magnitude can be achieved during laser pulses. This increase depends strongly on the shape of the electron velocity distribution.

These results were applied to the stimulated recombination of electrons and protons in electron cooling, and it was shown that this technique provides a unique tool to determine the longitudinal and transverse temperatures of a cooling electron beam.

If this method is applied in order to enhance the positron capture by antiprotons it would allow the production of antihydrogen atoms in a well-defined atomic state with a reasonable rate.

Acknowledgements

One of us (H.P.) wishes to thank the members of the electron cooling group of the Nuclear Physics Institute at Novosibirsk for fruitful and stimulating discussions during his stay at the Institute.

We thank Prof. G. zu Putlitz (Heidelberg) and Drs. H. Herr and D. Möhl (CERN) for fruitful discussions.

REFERENCES

[1] P. Lefèvre, D. Möhl and G. Plass, 11th Int. Conf. on High-Energy Accelerators, Geneva, 1980 (Birkhäuser Verlag, Basle, 1980), p. 819.

[2] L. Hütten, H. Poth, A. Wolf, H. Haseroth and Ch. Hill, The electron cooling device for LEAR, to be published in Proc. Workshop on Physics at LEAR with Low-Energy Cooled Antiprotons, Erice, May 1982 (ed. U. Gastaldi).

[3] G.I. Budker and A.N. Skrinsky, Sov. Phys.-Usp. 21, 277 (1978).

[4] M. Bell, J. Chaney, H. Herr, F. Krienen, P. Møller-Petersen and G. Petrucci, Nucl. Instrum. Methods 190, 237 (1981).

[5] H. Herr, D. Möhl and A. Winnacker, Production of and Experimentation with antihydrogen at LEAR, to be published in Proc. Workshop on Physics at LEAR with Low-Energy Cooled Antiprotons, Erice, May 1982 (ed. U. Gastaldi).

[6] Ya.S. Derbenev and A.N. Skrinsky, Part. Accel. 8, 235 (1978).

[7] M. Stobbe, Ann. Phys. (Germany) 7, 661 (1930).

[8] H. Bethe and E. Salpeter, Quantum mechanics of one- and two-electron systems, Handbuch der Physik (Springer, Berlin, 1957), Vol. 35, p. 88.

[9] P. Baratella, G. Puddu and F. Quarati, Z. Phys. A300, 263 (1981).

[10] L. Spitzer, Physics of fully ionized gases (Interscience, New York, 1956).

[11] M. Bell and J. Bell, Part. Accel. 12, 49 (1982), and references therein.

[12] G.I. Budker, N.S. Dikansky, V.I. Kudelainen, I.N. Meshkov, V.V. Parchomchuk, D.V. Pestrikov, A.N. Skrinsky and B.N. Sukhina, Part. Accel. 7, 197 (1976); Studies on electron cooling of heavy particle beams, CERN 77-08 (1977).

[13] V.V. Parchomchuk, private communication.

[14] B.R. Junker and J.N. Bardsley, Phys. Rev. Lett. 28, 1227 (1972);
W. Kolos, D.L. Morgan, D.M. Schrader and L. Wolhiewicz, Phys. Rev. A11, 1792 (1975);
R.I. Câmpaneu and T. Beu, Phys. Lett. 93A, 223 (1983).

[15] A.P. Mills, Appl. Phys. (Germany) 23, 189 (1980).

Figure captions

Fig. 1 : Schematic arrangement for electron cooling of stored ion beams.

Fig. 2 : Level scheme of a fully stripped ion in a cooling electron gas seen from the ion rest-frame.

Fig. 3 : Electron capture cross-section for capture into various atomic levels versus electron energy in units of E_0.

a) Cross-section for n = 1 states: —— σ_1 of Ref. 8 [see Eq. (2)]; --- σ_1 of Ref. 7 [see Eq. (A.1)].

b) Cross-section for n = 2 states: —— σ_2 of Ref. 8 [see Eq. (2)]; --- $\sigma_2 = \sigma_{2s} + \sigma_{2p}$; -·- σ_{2s}; -··- σ_{2p} of Ref. 7 [see Eq. (A.2)].

c) Cross-section for n = 3 states: —— σ_3 of Ref. 8 [see Eq. (2)]; --- $\sigma_3 = \sigma_{3s} + \sigma_{3p} + \sigma_{3d}$; -·- σ_{3s}; -··- σ_{3p}; -···- σ_{3d} of Ref. 7 [see Eq. (A.3)].

Fig. 4 : Concept for antihydrogen production [5] at the LEAR storage ring, using continuously stored and cooled positrons produced by an electron linac.

APPENDIX

The recombination cross-sections obtained by Stobbe [7] after calculating the hydrogenic bound-free matrix elements for main quantum numbers n = 1, 2, 3, of the bound states are given. The radial integrals result in terminating hypergeometric series, which determine the rational coefficients in the following formulae.

For n = 1, with $x = \sqrt{E_e/E_0}$:

$$\sigma_{1s} = A \cdot B_1(x) \cdot x^{-2} \cdot (1 + x^2)^{-2} \quad . \tag{A.1}$$

For n = 2, with $x = 2\sqrt{E_e/E_0}$:

$$\begin{aligned} \sigma_{2s} &= 8A \cdot B_2(x) \cdot x^{-2} \left[(1 + x^2)^{-2} + 3(1 + x^2)^{-3}\right] , \\ \sigma_{2p} &= 8A \cdot B_2(x) \cdot x^{-2} \left[3(1 + x^2)^{-3} + 8(1 + x^2)^{-4}\right] . \end{aligned} \tag{A.2}$$

For n = 3, with $x = 3\sqrt{E_e/E_0}$:

$$\begin{aligned} \sigma_{3s} &= 9A \cdot B_3(x) \cdot x^{-2} \left[3(1 + x^2)^{-2} + 32(1 + x^2)^{-3} + (208/3)(1 + x^2)^{-4} + (128/3)(1 + x^2)^{-5}\right] , \\ \sigma_{3p} &= 9A \cdot B_3(x) \cdot x^{-2} \left[24(1 + x^2)^{-3} + 208(1 + x^2)^{-4} + 224(1 + x^2)^{-5}\right] , \\ \sigma_{3d} &= 9A \cdot B_3(x) \cdot x^{-2} \left[(80/3)(1 + x^2)^{-4} + (736/3)(1 + x^2)^{-5} + 256(1 + x^2)^{-6}\right] . \end{aligned} \tag{A.3}$$

Here, $B_n(x) = \left[1 - \exp(-2\pi n/x)\right]^{-1} \exp\left[-(4n/x) \cdot \text{arc tg } x\right]$,

and $A = (2^8/3) \cdot \pi^2 \cdot \alpha\lambda_e^2$.

For $x \ll 1$, $B_n(x) \to e^{-4n}$. Then, the cross-sections depend on the kinetic energy of the incident electron as E_e^{-1}. As $1 + x^2 \approx 1$, the magnitude of the cross-sections is given by the sum of the rational coefficients.

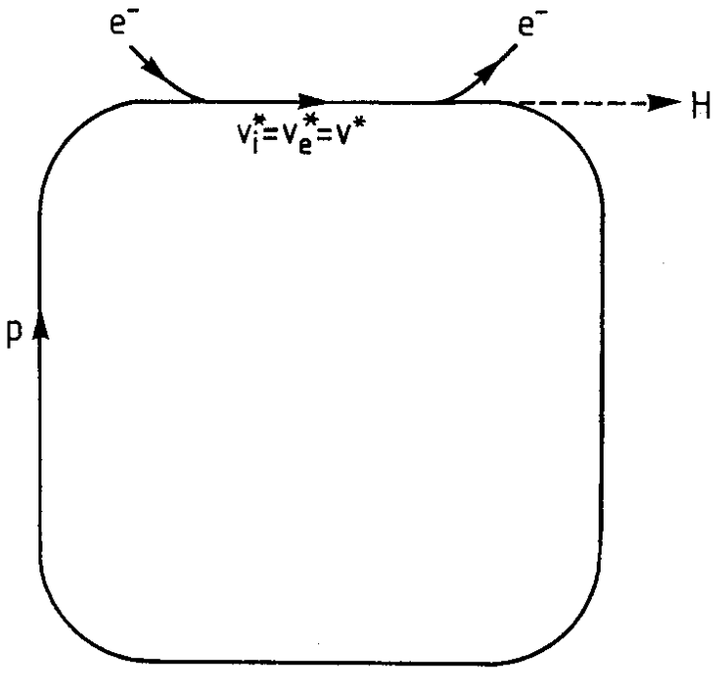

Fig. 1

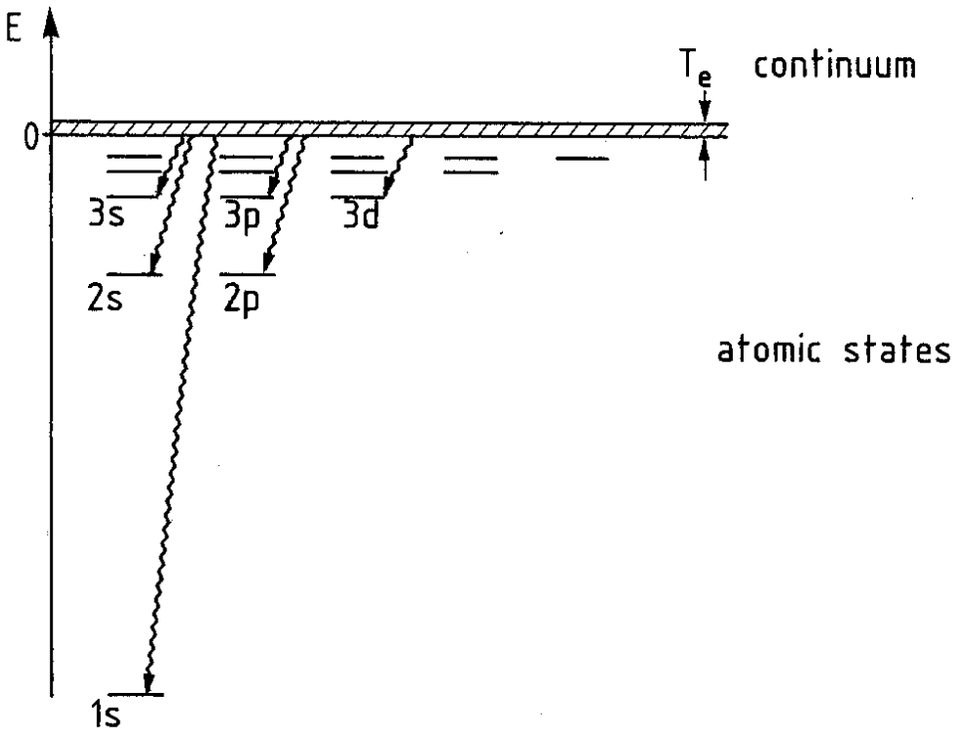

Fig. 2

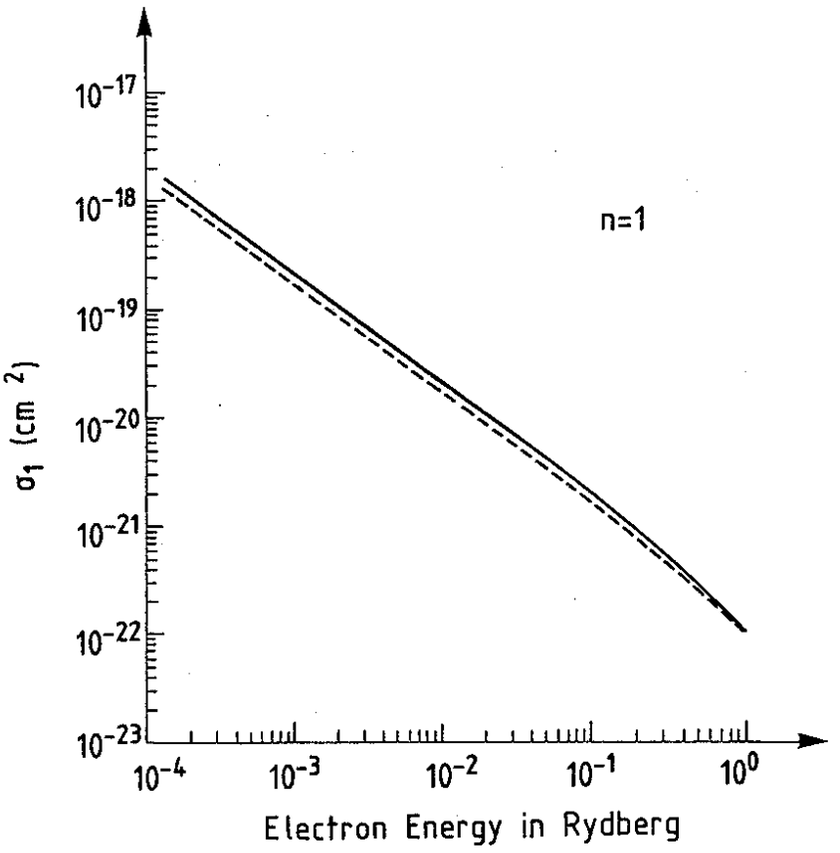
n=1
σ_1 (cm^2)
10^{-17}
10^{-18}
10^{-19}
10^{-20}
10^{-21}
10^{-22}
10^{-23}
10^{-4}
10^{-3}
10^{-2}
10^{-1}
10^{0}
Electron Energy in Rydberg

Fig. 3 a)

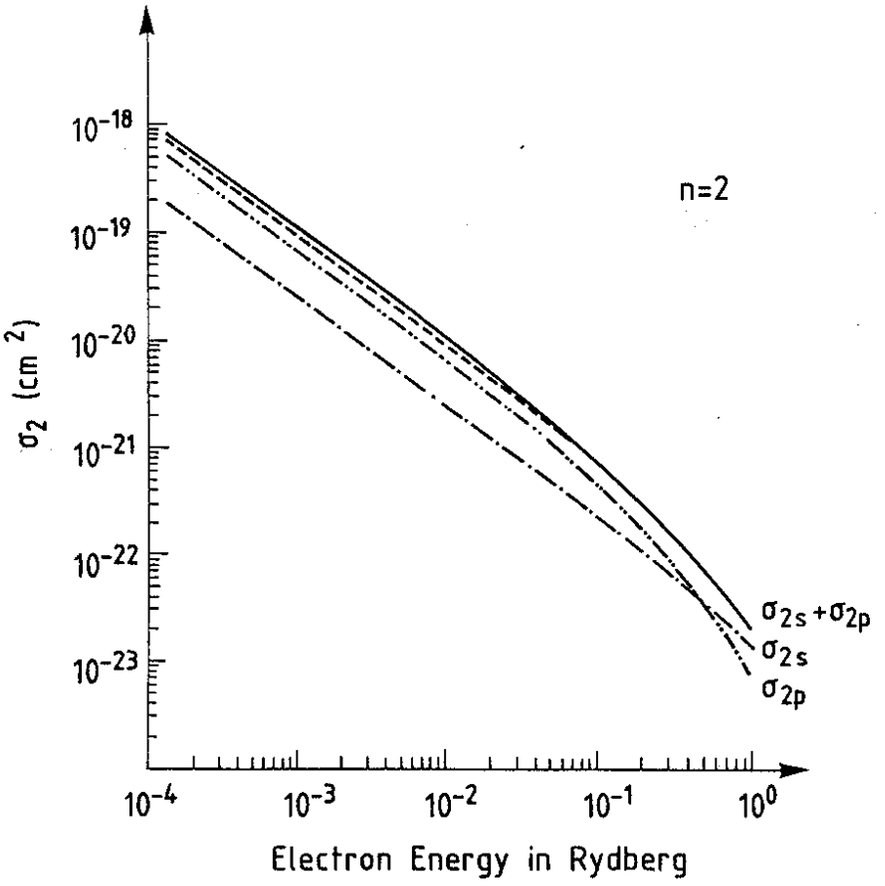
n=2
σ_2 (cm^2)
10^{-18}
10^{-19}
10^{-20}
10^{-21}
10^{-22}
10^{-23}
$\sigma_{2s}+\sigma_{2p}$
σ_{2s}
σ_{2p}
10^{-4}
10^{-3}
10^{-2}
10^{-1}
10^{0}
Electron Energy in Rydberg

Fig. 3 b)

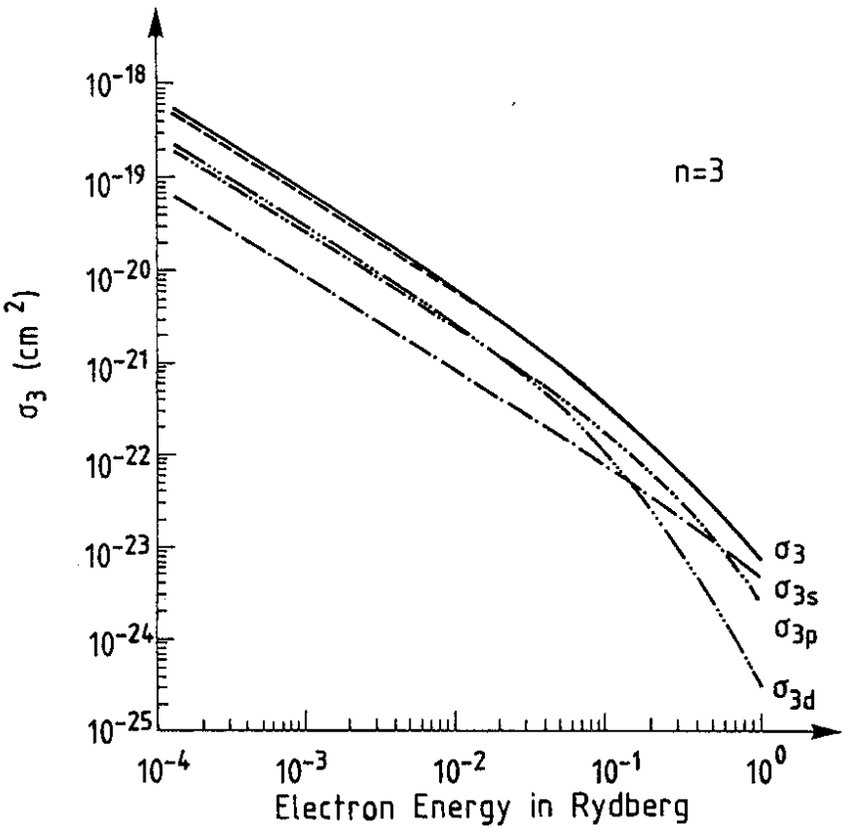
n=3
σ_3
σ_{3s}
σ_{3p}
σ_{3d}
σ_3 (cm^2)
10^{-18}
10^{-19}
10^{-20}
10^{-21}
10^{-22}
10^{-23}
10^{-24}
10^{-25}
10^{-4}
10^{-3}
10^{-2}
10^{-1}
10^{0}
Electron Energy in Rydberg

Fig. 3 c)

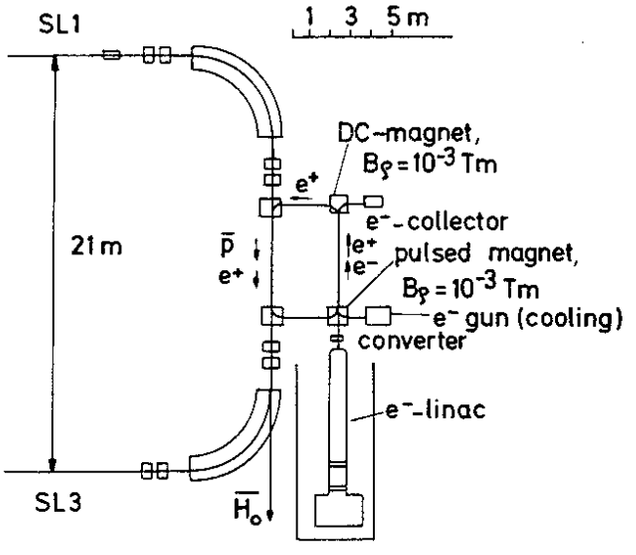
SL1
1 3 5 m
DC-magnet,
$B\rho = 10^{-3}$ Tm
e^+
e^--collector
21 m
$\bar{p}$
e^+
e^+
e^-
pulsed magnet,
$B\rho = 10^{-3}$ Tm
e^- gun (cooling)
converter
e^--linac
SL3
$\bar{H}_o$

Fig. 4